Article

Deriving Ice Motion Patterns in Mountainous Regions by Integrating the Intensity-Based Pixel-Tracking and Phase-Based D-InSAR and MAI Approaches: A Case Study of the Chongce Glacier

Shiyong Yan [1], Zhixing Ruan [2], Guang Liu [2,*], Kazhong Deng [1], Mingyang Lv [2] and Zbigniew Perski [3]

1. Jiangsu Key Laboratory of Resources and Environmental Engineering, School of Environment Science and Spatial Informatics, China University of Mining and Technology, Xuzhou 221116, China; yan_shiyong@126.com (S.Y.); kzdeng@cumt.edu.cn (K.D.)
2. Key Laboratory of Digital Earth Science, Institute of Remote Sensing and Digital Earth, Chinese Academy of Sciences, Beijing 100094, China; ruanzx@radi.ac.cn (Z.R.); lmynju@163.com (M.L.)
3. Polish Geological Institute—National Research Institute, Carpathian Branch, Cracow 31560, Poland; zper@pgi.gov.pl
* Correspondence: liuguang@radi.ac.cn; Tel.: +86-10-8217-8177

Abstract: As a sensitive indicator of climate change, mountain glacier dynamics are of great concern, but the ice motion pattern of an entire glacier surface cannot be accurately and efficiently generated by the use of only phase-based or intensity-based methods with synthetic aperture radar (SAR) imagery. To derive the ice movement of the whole glacier surface with a high accuracy, an integrated approach combining differential interferometric SAR (D-InSAR), multi-aperture interferometry (MAI), and a pixel-tracking (PT) method is proposed, which could fully exploit the phase and intensity information recorded by the SAR sensor. The Chongce Glacier surface flow field is estimated with the proposed integrated approach. Compared with the traditional SAR-based methods, the proposed approach can determine the ice motion over a widely varying range of ice velocities with a relatively high accuracy. Its capability is proved by the detailed ice displacement pattern with the average accuracy of 0.2 m covering the entire Chongce Glacier surface, which shows a maximum ice movement of 4.9 m over 46 days. Furthermore, it is shown that the ice is in a quiescent state in the downstream part of the glacier. Therefore, the integrated approach presented in this paper could present us with a novel way to comprehensively and accurately understand glacier dynamics by overcoming the incoherence phenomenon, and has great potential for glaciology study.

1. Introduction

Glaciers have been recognized as an indicator of climate change by the scientific community as their dynamics are extremely sensitive to variations in precipitation and temperature. Characterized by steep terrain and a relatively small size, mountain glaciers located at low latitudes, such as high-mountain Asia, are much more sensitive to global climate change than glaciers in polar regions [1–3]. The intense activity of mountain glaciers can also present the potential for danger due to the rapid ice movement [4,5]. Mountain glaciers can also be valuable sources of fresh water, and directly impact human livelihoods, infrastructure security, and water levels [6–8].

The precise monitoring of glacier extent, mass balance, and surface velocity therefore plays a key role in determining the glacier status, and can provide critical information describing the dynamics of mountain glaciers in response to climate change [9–11]. Among these characteristics, ice movement is one of the most important parameters for assessing a shift in equilibrium because the acceleration or deceleration of ice motion is synonymous with changes in glacier balance and flow dynamics [4,12]. Ice displacement monitoring can help us obtain improved knowledge on the response of glaciers to global climate change [1,2,10,13]. Thus, monitoring the movements of mountain glaciers is of great importance, and it is particularly important to monitor the whole glacier surface with a high degree of accuracy [14–16]. Unfortunately, in situ measurement is not appropriate for the investigation of mountain glacier motion in remote regions, because it is costly and time-consuming, or may even be impossible, and is usually accompanied by danger [17–19].

Characterized by being independent of cloud cover and solar illumination, synthetic aperture radar (SAR) operating at long wavelengths, such as L-band and C-band, has provided an invaluable way to detect and measure mountain glacier motion [20,21]. Compared with optical imagery and in situ surveys, it has been successfully exploited to detect glacier motion in a number of previous studies, usually with differential interferometric SAR (D-InSAR) [22–24] and pixel-tracking (PT) methods [10–12]. Furthermore, multi-aperture interferometry (MAI) has also been proposed and employed to estimate ice velocity on glacier surfaces in recent years [23,25,26].

However, D-InSAR and MAI measurements are significantly affected by the incoherence phenomenon caused by the large temporal baseline and the high motion gradient associated with the rapid ice velocity [10,25,27], which results in SAR interferometry failing when it is used to observe glaciers in mountainous areas, especially in the sections with rapid motion. The PT technique is considered to be the best alternative method of determining ice motion with SAR intensity information, although it is subject to low accuracy. However, it is not usually affected by the decorrelation phenomenon and can be applied to SAR image pairs with a long temporal interval and used on glacier surfaces with a high velocity [5,11,27]. In order to exploit the advantages of different approaches with SAR imagery, the synergistic approach of InSAR and speckle-tracking has been proposed and applied for monitoring the complex surface deformation caused by the landslide and mining activities [28–30]. Although time series deformation extraction based on analysis of both phase and amplitude information of SAR imagery is only in one direction, it has obviously presented the benefits of integrated method. Nevertheless, there have been few studies of glacier motion in mountainous regions using a single SAR imagery pair and integrating the D-InSAR, MAI, and PT approaches.

In this paper, we propose an integrated strategy based on comprehensive utilization of the phase information (D-InSAR and MAI) and intensity information (pixel tracking) of spaceborne SAR imagery, which is used to yield an accurate and detailed ice motion pattern for the Chongce Glacier in the West Kunlun Mountains, China, by fully exploiting the SAR imagery. Unfortunately, the motion decomposition operation with one-path SAR data usually needs the strong assumption of ice flow parallel to the glacier surface, which may not conform to reality. Furthermore, the error of DEM and imaging geometry would present the additional error in the ice motion after the decomposing operation. In order to avoid the error introduced by the motion decomposition operation, the derived ice motion is therefore presented in the SAR imaging dimension composed of the along-track and slant-range directions. The Shuttle Radar Topographic Mission (SRTM) digital elevation model (DEM) at 3 arc second resolution is employed to remove and compensate for the topography-related signal in the D-InSAR, MAI, and PT methods [5,31,32].

2. Study Area and Datasets

2.1. Study Area

The Chongce Glacier is located in the eastern part of the West Kunlun Mountains, China, and is one of the most densely concentrated regions of mountain glaciers in the Tibetan Plateau. With a length of 27 km and a maximum width of 3 km (Figure 1), the Chongce Glacier is one of the most

famous glaciers in the region. Due to its great thickness and size, an ice core was extracted from the upstream part of the Chongce Glacier in the 1980s, giving us the opportunity to study the relationship between historical climate change and ice development. Most of the glacier surface is clean ice or snow cover, except for the glacier terminus, which is covered by debris. In addition, foliation and crevasses caused by the intense ice activity on the glacier surface are also common, and can be clearly observed in Figure 1.

The climate of the study area is monsoon-dominated, and most of the annual precipitation falls during the monsoon season from June to September, which is also the ice ablation season. The annual temperature and precipitation are respectively about −14 °C and 300 mm around the glacier equilibrium-line altitude (ELA), which is located at 5930 m above sea level (a.s.l) [33,34]. The shrinkage or extension of the Chongce Glacier has only been rarely observed with moderate spatial resolution Landsat imagery over the past decades [7,35]. Thus, the glacier status cannot be immediately determined by the traditional optical imagery-based interpretation method, which only gives information about the area. The low correlation between glacier area variation and the status of the ice over a short time scale means that study of the surface motion of the ice is required to obtain a better indication of the ice status [36]. Therefore, in addition to the variation of the glacier edges, the ice activity on the entire glacier surface is efficiently reflected by the integrated method presented in this paper. Although previous studies have employed Envisat and Advanced Land Observation Satellite (ALOS) SAR pairs to estimate ice surface motion at a large scale with the PT technique [10], this study presents a much more accurate and detailed surface motion field for the Chongce Glacier, based on the integration of the D-InSAR, MAI, and PT approaches.
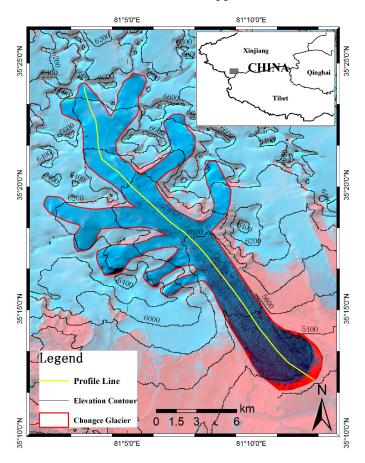

Figure 1. Landsat-5 image of Chongce Glacier in the West Kunlun Mountains. The translucent mask was employed on the surrounding mountain area for highlighting the study area, which is outlined with the red line. The red area means the surrounding non-glacial mountain area. Both the light-blue and dark-blue are the ice or snow coverage, respectively. The location is indicated in the inset.

2.2. Datasets

In this paper, ALOS Phased Array L-band Synthetic Aperture Radar (PALSAR) images are employed to determine the ice motion of the Chongce Glacier, because the L-band SAR data can maintain coherence for a much longer time due to the deep penetration of ice. Compared with C- and X-band data, L-band PALSAR images have been used in many glacial regions and are capable of giving an accurate and complete coverage estimation for moving ice at a large scale [5,9–11]. Details of the PALSAR imagery pair used in this paper are listed in Table 1. All ice displacements presented in the following figures occurred during the temporal interval between the two SAR acquisitions.

Table 1. Details of the ALOS/PALSAR imagery pair.

Date	B//	B⊥	Path	Frame	Temporal Baseline
DEC-13-2008	144 m	299 m	515	690	46 days
JAN-28-2009					

3. Method

The integrated method is used to determine the ice motion on the entire glacier surface with a relatively high accuracy. It efficiently exploits the phase information by the D-InSAR and MAI methods and the intensity information by the PT technique, aiming to minimize the noise and errors, as well as improve the accuracy of ice motion measurement, along with maximizing the glacier surface coverage. Not only the significant ice motion in the upper and middle sections of the glacier, but also the small amount of ice movement in the glacier terminus part can also be accurately determined by the integrated method, which can be considered as an upgraded version of SAR utilization.

3.1. Phase-Based Methods: D-InSAR and MAI

D-InSAR and MAI are two popular approaches for investigating surface deformation based on the phase information of SAR imagery. The satellite-based repeat-pass D-InSAR observations are the most widely used method for detecting and assessing the movement of glaciers with a large spatial coverage, because of the development of the related algorithms and the ever-increasing SAR data archive [37]. In this paper, D-InSAR is applied to process the PALSAR data of the descending orbit covering the target glacier. SRTM DEM data is used to remove the topographic phase contribution after applying an azimuth common band filter and a range spectral shift filter to suppress the decorrelation noise [38]. The interferogram is then generated with a multi-look operation of four looks in the range, and 12 looks in the azimuth, direction, respectively, followed by the improved adaptive Goldstein interferogram filter to improve the fringe quality [39]. SNAPHU software is employed to obtain the unwrapped phase with the corresponding coherence file [40], which can improve the quality and accuracy of the unwrapping operation by masking out the low coherence regions. The displacement in the line-of-sight (LOS) direction can then be computed as follows [22]:

$$\delta_{LOS} = -\frac{\phi_{LOS} \cdot \lambda}{4\pi} \tag{1}$$

where δ_{LOS} is the ice displacement in the slant-range direction, ϕ_{LOS} is the corresponding unwrapped phase, and λ is the SAR wavelength. For L-band PALSAR data, λ is 23.6 cm.

In addition to D-InSAR, MAI is another phase-based approach which can exploit the interferometric phase to estimate the surface displacement along the azimuth direction [23,26,41]. When combined with the D-InSAR approach, the motion pattern of the glacier can be obtained in two-dimensional coordinates composed of the slant-range and along-track directions. In addition, when compared with the PT technique, the azimuth displacement measurements can be improved by the MAI approach to a certain extent [23,26]. However, MAI and the D-InSAR technique can usually

be successfully used only in regions with a high coherence. Their utilization is thus often seriously limited by the incoherence phenomenon occurring on the glacier surface.

In MAI processing, the single-look complex (SLC) images are first processed by the azimuth common band filtering with a squint of half an aperture to generate sub-aperture SLC images [42]. The sub-aperture SLC images are then used for generating forward- and backward-looking differential interferograms by the repeat-orbit D-InSAR approach. The along-track displacement can then be finally retrieved from the phase differences between the forward- and backward-looking differential interferograms. The relationship between the across-track motion and the MAI interferometric phase can be defined as follows [23,25]:

$$\delta_{MAI} = -\frac{\phi_{MAI} \cdot l}{4\pi n} \tag{2}$$

where δ_{MAI} is the azimuthal movement of the glacier surface, ϕ_{MAI} is the corresponding unwrapped phase, l is the effective antenna length, and n is a normalized squint that is a fraction of the full aperture width. For PALSAR, l = 8.9 m, and one fringe yields 8.9 m if n = 0.5 is used. From the equation, it can be seen that the sensitivity to surface motion is lower than that of the D-InSAR technique due to the relatively long wavelength [23].

3.2. Intensity-Based Method: PT

Compared with SAR interferometry techniques, the PT method can overcome the low coherence caused by the large spatial/temporal baseline and the limitation of the maximum detectable deformation of SAR interferometry [10,43]. It is based on the intensity information, which is obtained along with the phase information recorded by SAR imagery. A distinctive superglacial pattern on the glacier surface can be efficiently tracked by the PT method in multi-temporal SAR images to determine the glacier surface motion. The ice motion related offset signal is usually estimated by removing the whole trend of the motion (i.e., the long wavelength signal) associated with the orbit and sensor attitude from the results of the SAR imagery matching operation. Before being converted to ice motion, the topographic-dependent distortion associated with the rugged terrain in mountainous glacial areas and the residual trend should be compensated for and removed with the DEM-assisted method followed by a linear polynomial model [5,44]. In order to generate reasonable results, a filter is usually employed on the magnitude and flow direction of the obtained motion field. Compared with motion estimated in only one direction (i.e., with MAI or D-InSAR), the PT approach can simultaneously present the displacement in both the along- and across-track directions [10,12,27]. It has been proved that the PT method could obtain the ice motion on a whole glacier surface, especially on the parts with large movements during the period between SAR acquisitions. Therefore, SAR intensity based PT may be the most appropriate approach to determine rapid ice movement in mountainous regions [15,31].

3.3. The Integrated D-InSAR, MAI, and PT Strategy

Due to the different operation mechanisms, the continuity and accuracy of SAR interferometry, especially D-InSAR, is much better than that of PT, but PT is still valuable, especially for regions with rapid ice motion or low coherence. To fully explore and exploit the respective advantages of the D-InSAR, MAI, and PT approaches, an optimal integrated strategy is presented. The corresponding data processing flowchart is shown in Figure 2.
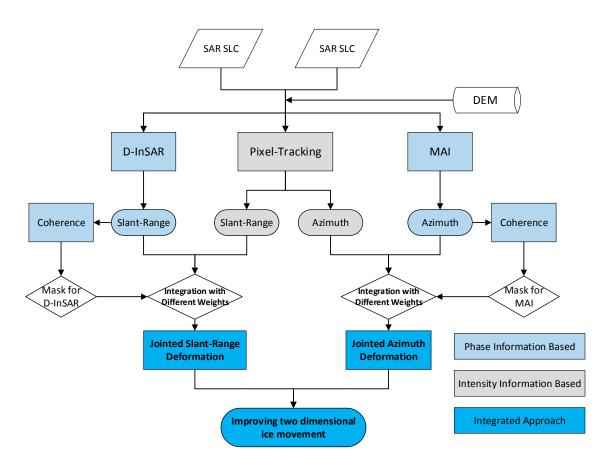
Figure 2. The data processing flowchart of the integrated method.

Most of the previous studies have used only one or two of the previously mentioned methods based on SAR imagery [10,37,41], but few have taken both the phase and intensity information contained within SAR data to determine ice motion, especially in mountainous areas with complex terrain. In this paper, the results of the three methods are first presented separately. We then present and optimize the integrated operation based on the respective procedures to obtain an accurate ice velocity pattern covering the mountain glacier surface. The accuracy can also be partly proved by a comparison of the respective results of the D-InSAR, MAI, and PT techniques in a common region on the glacier surface, especially in slow-flowing ice areas. Therefore, the robustness of the spaceborne SAR-based ice motion determination method can be improved by integrating the phase and intensity information based approaches.

The masks generated from the coherence files (Figure 3) are used to integrate both results as the main determining factors, which control the combined operation and determine the weight of the phase result and the intensity result in the final ice motion estimation. Clearly, the weight of the D-InSAR and MAI measurements are expected to be higher than that of PT since the interferometric phase is generally much more accurate than the intensity in the detection of displacement, despite the fact that they are less robust than the PT method [2,12,15,43]. In addition, once the absolute difference value between the D-InSAR/MAI and PT results is greater than the threshold, the ice measurement from PT dominates the final glacier movement in the corresponding overlapping region. The general principle used in this study is shown in Equation (3), where the parameters are experientially given according to the above principle and the experiments. Furthermore, in order to ensure the continuity of

the ice displacement, the overlapping region between results can be used for validation and calibration of the ice motion estimation of the different mechanisms.

$$m_t = \begin{cases} m_{ph} & coh > 0.7 \\ m_{in} & coh < 0.3 \\ 0.9m_{ph} + 0.1m_{in} & \quad if \quad \quad 0.3 < coh < 0.7 \\ 0.15m_{ph} + 0.85m_{in} & 0.3 < coh < 1 \ \& \ \left| m_{ph} - m_{in} \right| > 0.5m \end{cases} \tag{3}$$

where m_{ph} and m_{in} are respectively the motion from the phase and intensity information of the SAR imagery, m_t is the obtained final motion, and *coh* is the corresponding coherence value on the glacier surface.
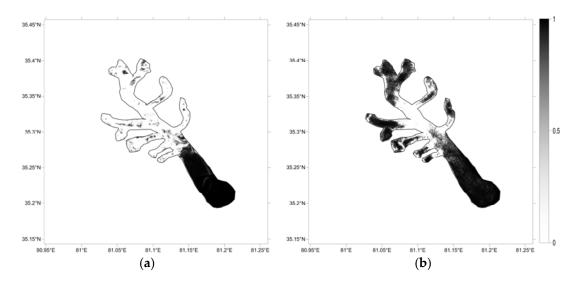

Figure 3. Coherence distribution on the Chongce Glacier. (**a**) Coherence for D-InSAR; (**b**) Coherence for MAI.

3.4. Accuracy Estimation and Error Analysis

The accuracy of the D-InSAR approach has been widely proved in previous studies of precise movement extraction [20,22]. According to the D-InSAR result, the accuracy of the PT method can also be ensured because of the existing overlapping region. In addition, the accuracy of the PT method can be statistically yielded by the residual values on the non-glacial area, which are computed according to the basic principle of the PT method as it is a relative measurement technique [5,22,42]. The statistical values in non-glacial region for results of D-InSAR, MAI, and PT methods area are, respectively, 0.09 m, 0.34 m, and 0.5 m, which could be considered as their accuracies. By the same way, the accuracy for the ice motion field obtained by the integrated method is about 0.2 m. However, due to the different dominated approaches on different parts of the glacier surface, the local accuracy on the section with slow ice motion is usually larger than that with the large ice motion. Generally speaking, the relative accuracy has been improved by the integration operation.

From Figure 4, it can be seen that the accuracy of D-InSAR and MAI is better than that of the PT method in the area with high coherence. It can also be seen in Figure 5 that the correlation is high in the overlapping region between the respective results of D-InSAR, MAI and PT. Both Figures 4 and 6 reveal that the results of the different approaches correctly reflect the general ice motion trend, but the measurement accuracy of D-InSAR is generally better than that of both the MAI and PT methods. In addition, it can be clearly observed in Figures 4 and 5 that the accuracy of MAI could not be much higher than that of the PT technique because of its relatively long antenna length. The statistical characteristic of the residual values on the non-glacial region has proved this visual

interpretation. However, the MAI result is much more continuous, despite being seriously limited by the low coherence on some parts of the glacier surface. In addition, the statistical characteristic of the residual value on the non-glacial area can also be computed for accuracy estimation of the integrated method, according to the basic relative measuring principle of an integrated method [4,5].
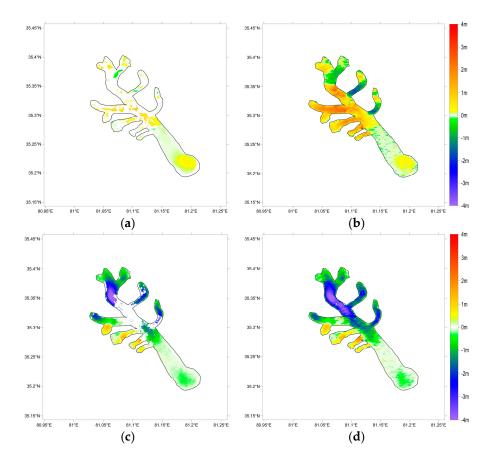
Figure 4. Results of D-InSAR, MAI, and PT during the temporal period of 23 December 2008–28 January 2009. (**a**) D-InSAR unwrapping result; (**b**) PT result in the LOS direction; (**c**) MAI unwrapping result; and (**d**) PT result in the along-track direction.
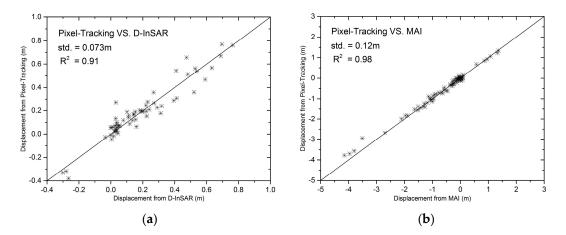
Figure 5. Correlation between D-InSAR/MT and PT in the overlapping region. (**a**) PT vs. D-InSAR; and (**b**) PT vs. MAI.
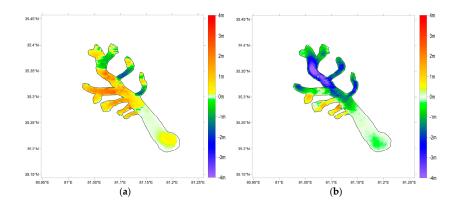
Figure 6. The integrated result of D-InSAR, MAI, and PT. (**a**) D-InSAR and PT in the across-track direction; and (**b**) MAI and PT in the along-track direction.

4. Results and Analysis

4.1. Integrated Result

Following the data processing flowchart of SAR interferometry, the interferogram and corresponding coherence are obtained with four looks in the range direction and 12 looks in the azimuth direction to obtain results in an appropriate proportion. The parameters for both the PT operation and SAR interferometry are carefully selected. The sample interval window is four pixels and 12 pixels in the range and azimuth directions, respectively. Therefore, the results are in the same geometric grid on the Chongce Glacier surface. In addition, the size of the search window and sample window are experimentally chosen to obtain the optimal results for the target glacier.

The D-InSAR and MAI coherence maps in Figure 3 are used as the weight factors for deciding the roles of D-InSAR, MAI, and PT in the final result. A low coherence value usually means that the ice motion is much more dependent on the PT method; otherwise, a high coherence value means that the ice motion is much more dependent on the SAR interferometry. When the coherence is lower than the given threshold, only the result of the PT method is used because of the serious decorrelation phenomenon of D-InSAR and MAI. The joint results in the slant-range and azimuth directions are shown in Figure 6.

In addition, according to the R-squared statistics in Figure 5 between the phase-based and intensity-based methods, the different methods generally yield results that agree well with each other. Compared with the previous studies [5,10], a much more accurate ice motion is presented in the final ice flow pattern maps in both Figures 6 and 7. The detailed motion information is also much clearer in the final results generated in this paper. The characteristics of the ice motion are, thus, clearly indicated by the accurate results, especially on the terminus of the glacier, which features a low velocity. For the purpose of a more quantitative analysis, the profile of the glacier velocity along the approximate central flow line on the glacier surface, as well as the slopes, is plotted in Figure 8. The slopes' values are presented along the profile in different parts with different ice motion characteristics. Here, it can be observed that the spatial distribution of the glacier movement is not closely related to the terrain elevation profile and the slopes in Figure 8. In general, motion on the original part of the Chongce Glacier is slow, and then quickly increases with decreasing elevation, until reaching 6200 m a.s.l. The ice flow then slows down until it becomes nearly stable in the 10 km before the terminus. The ice on the glacier surface between 5 km and 10 km from the terminus is almost in a quiescent phase. Then, along with the decreasing elevation, the ice motion begins to increase slowly again, reaching about 0.5 ± 0.04 m on the glacier terminus during the period of SAR imagery acquisition. The part with the maximum motion detected on the glacier surface appears in the upper section of the Chongce Glacier at an elevation of 6200 m a.s.l, where the ice flows at about 4.9 ± 0.2 m over the 46 days.
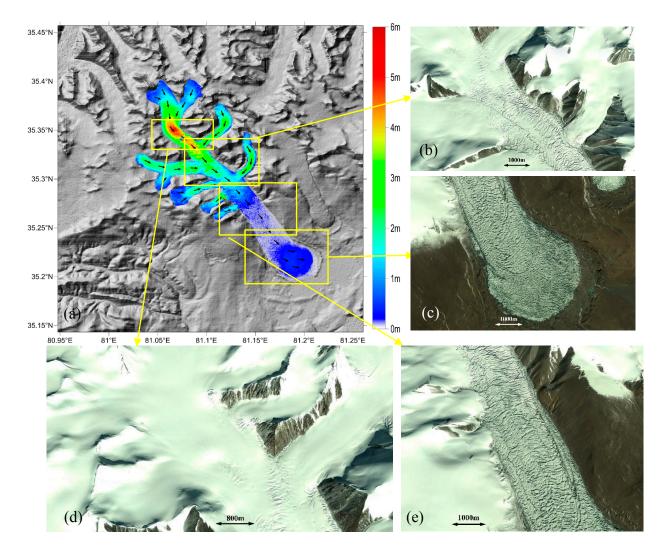
Figure 7. The Chongce Glacier flow field generated by the integrated method. (**a**) The ice motion pattern superimposed on the DEM data; and (**b–e**) optical images from WorldView-2 mosaic image corresponding to different parts of the Chongce Glacier surface.
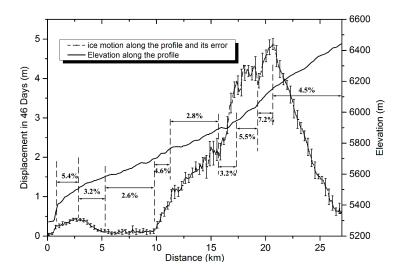

Figure 8. Ice motion and elevation profiles along the central line of the Chongce Glacier surface and percentages marked between two dotted lines are the slopes of the terrain in corresponding sections.

4.2. Ice Motion Pattern

The final motion pattern covers the entire glacier surface with a relatively high accuracy by utilizing the proposed approach. With the help of the combined method, the ice velocity during the period between SAR imagery acquisitions can be precisely reflected by the integrated method. The final ice motion field also reflects the velocity variation in the intersection between the main trunk glacier and its tributaries, which can also be proved by the patterns of the foliation and crevasses on the glacier surface in Figure 7b–d.

According to the ice motion in Figure 7, the exchange of ice mass can be clearly reflected by the motion field, which can be considered as a useful proxy for assessing glacier mass balance [9,23]. Thus, the pattern of the ice mass exchange strength on the glacier surface can also be clearly reflected in the final ice motion field. From Figure 7, the ice motion reaches a maximum in the section where the exchange of ice mass is much more intensive than elsewhere. In the downstream section, the velocity is generally much lower than that of the upstream part. After the approximately 5 km length of stable ice region in the downstream part, the ice movement becomes intense again on the glacier terminus, which is clearly and accurately detected by the integrated method. Due to the relatively low elevation, ice ablation of the Chongce Glacier mainly occurs in the downstream part, especially at the terminus of the glacier. The ice flowing into this section from the upstream part, along with the low temperature, plays a positive role in preventing serious retreat of the Chongce Glacier. Therefore, over the past decades, the position of the terminus of the Chongce Glacier has remained relatively stable, while most of the mountain glaciers in Tibet are suffering from ablation and retreat because of global warming.

5. Discussion

5.1. Integrated Method Analysis

From the previous studies [10,22], it can be seen that relatively large movements are best covered by the intensity-based PT method, while small movements of the glacier surface can be accurately and efficiently detected by the phase-based D-InSAR or MAI approaches. Therefore, an ice motion field covering the entire glacier should be computed by the appropriate methods on different parts of the glacier surface because of the wide range of ice motion. Only in this way can the accuracy of the result be improved by fully exploiting the information and advantages of SAR imagery and the SAR-based methods. The whole glacier surface can be covered by the presented method with a relatively high accuracy, even in the invalid regions of D-InSAR and MAI caused by the decorrelation factors. Thus, the integrated method has great potential for detecting mountain glacier movement in complex terrain, where the ice flow velocity usually varies over a large range and high coherence is no longer necessary. However, the proposed method is not as accurate as D-InSAR, but it is significantly more accurate than the PT method, especially in the regions with small movements, due to the different operating mechanisms in different sections.

The overlapping region of the phase-based and intensity-based results gives us an opportunity to validate the accuracy of the results generated by the different methods. The highly-accurate glacier surface motion observation is an excellent way to better understand the glacier motion pattern, ice dynamics, and development. With the accurate ice motion field, an ice flow related disaster could be efficiently and precisely predicted. Thus, the integrated method is a useful way to cover regions with both low and high ice velocities. With this approach, the ice motion in mountainous regions can be much more efficiently estimated during the ablation or accumulation period by completely covering the ice surface of the entire glacier.

5.2. Ice Motion Characteristics

In general, ice motion is greatly affected by many factors, including climate condition, the local terrain, the ice mass gravity force and so on. However, it could be seen in Figure 8 that the topography and corresponding terrain slope along the profile is not well correlated with the ice motion on the

glacier surface, which probably means that the terrain was not the determining factor affecting the ice movement of Chongce Glacier and its discussion is out of the scope of this paper. In fact, the quiescent state and slow motion of the ice in the downstream part result in the glacier terminus being dome-shaped (see Figures 1 and 7). In addition, the foliation and crevasses development on the glacier surface is obviously caused by the ice motion change. It can be seen that foliation and crevasses are developed well on the sections with intense ice speed variation, which partly proved that the obtained ice motion field is closely related to the glacier dynamics. With the detail and accuracy ice motion field we could predict the foliation and crevasses development on glacier surface, which would be helpful in studying glacier stress and strain.

The ice slows down from the upper part to the downstream part until reaching the glacier terminus. The maximum motion appears in the upper part of the Chongce Glacier, rather than the middle part and the terminus. Clearly, it can be seen from Figures 7 and 8 that there are about 5 km in the downstream part which show little movement, which is followed by the terminus with increased movement. Additionally, ice motion is not a constant across the glacier and usually reaches the maximum along the central line because of the friction of glacier's bed and valley walls. Thus, both friction resistance from the surrounding terrain and the counterforce from the downstream ice may be the main factors slowing down the ice and forming the presented glacier surface motion pattern. Furthermore, the foliation and crevasses on the glacier surface observed in the high-resolution optical imagery (see Figure 7) may be caused by the extrusion (ice uplift) and cracking associated with intense ice motion. The foliation and crevasses mainly appear in the middle and downstream parts of the Chongce Glacier because of the motion associated with the ice mass variation, while the ice surface is mainly covered by snow in the upstream part. Therefore, the ice motion variation can result in some features (such as crevasses) on the glacier surface, which can be used to reflect the glacier dynamics in mountainous regions. This phenomenon was also observed in a previous study of the SAR-based PT method [10].

There is little area variation observed in the Chongce Glacier terminus during the period of SAR acquisitions. However, the low ablation and motion of the ice results in slight surface deformation because of the relatively high temperature on the glacier terminus and the relatively low elevation. Thus, the value of the integrated motion measurements are greatly emphasized by determining the ice motion on the entire glacier surface, rather than just using the ice area variation. Furthermore, the slight deformation occurring on the glacier terminus and the downstream part detected by SAR interferometry may not be caused by only the ice motion, but also its ablation, because of the relatively high temperature in the low elevation area when compared to other parts of the glacier. In summary, the high accuracy of the integrated method can directly reflect the details of the ice motion, which will be of great help when studying and predicting ice flow and understanding glacier dynamics.

6. Conclusions

A relatively high-accuracy ice motion pattern covering the entire Chongce Glacier surface is obtained by the proposed approach integrating the D-InSAR, MAI, and PT techniques. Based on the intensity and phase information, the integrated method not only fully exploits the employed SAR imagery to reveal an accurate glacier motion pattern, but also extends the scope of the SAR application in extracting ice motion in large-scale regions with a wide range of ice flow velocities.

The observed values in common regions can be used to validate and calibrate the motion generated by the different methods to ensure a better combined operation. The high correlation between D-InSAR/MAI and PT in the common region proves the validation of the integrated method. A visual interpretation of final complete spatial coverage of ice motion reveals large differences between the motions measured on the different sections of the glacier surface. Since these differences are beyond the estimated errors, we can assume that they accurately depict the actual changes in glacier motion, especially on the terminus part, where the ice motion was not given in previous studies.

The measurements also give us a deep insight into the complex motions of the surface of the Chongce Glacier. The improved accuracy will be useful when capturing and studying ice activity under climate warming. It will also be much more useful than the other methods in predicting ice motion-related disasters, because of its relatively high accuracy. Therefore, the integrated approach presented in this paper has great potential for glaciology studies and give us a novel way to understand glacier variations. However, the mechanism of the mass gain and glacier surge in the Chongce Glacier, as well as the rest of the West Kunlun Mountains region, requires further study by the presented integrated approach.

Author Contributions: Guang Liu and Shiyong Yan conceived and designed the experiments; Shiyong Yan and Zhixing Ruan performed the experiments; Kazhong Deng, Zbigniew Perski and Mingyang Lv analyzed the results; Shiyong Yan and Zhixing Ruan wrote the paper.

Conflicts of Interest: The authors declare no conflict of interest.

Abbreviations

D-InSAR	differential interferometric synthetic aperture radar
MAI	multi-aperture interferometry
PT	pixel tracking
SRTM	Shuttle Radar Topography Mission
DEM	digital elevation model
SNAPHU	Statistical-Cost, Network-Flow Algorithm for Phase Unwrapping
ALOS	Advanced Land Observing Satellite
PALSAR	Phased Array type L-band Synthetic Aperture Radar

References

1. Haeberli, W.; Hoelzle, M.; Paul, F.; Zemp, M. Integrated monitoring of mountain glaciers as key indicators of global climate change: The European Alps. *Ann. Glaciol.* **2007**, *46*, 150–160. [CrossRef]

2. Hu, J.; Li, Z.-W.; Li, J.; Zhang, L.; Ding, X.-L.; Zhu, J.-J.; Sun, Q. 3-D movement mapping of the alpine glacier in Qinghai-Tibetan plateau by integrating D-InSAR, MAI and Offset-Tracking: Case study of the Dongkemadi Glacier. *Glob. Planet. Chang.* **2014**, *118*, 62–68. [CrossRef]

3. Immerzeel, W.W.; Kraaijenbrink, P.D.A.; Shea, J.M.; Shrestha, A.B.; Pellicciotti, F.; Bierkens, M.F.P.; de Jong, S.M. High-resolution monitoring of Himalayan Glacier dynamics using unmanned aerial vehicles. *Remote Sens. Environ.* **2014**, *150*, 93–103. [CrossRef]

4. Necsoiu, M.; Onaca, A.; Wigginton, S.; Urdea, P. Rock glacier dynamics in Southern Carpathian Mountains from high-resolution optical and multi-temporal SAR satellite imagery. *Remote Sens. Environ.* **2016**, *177*, 21–36. [CrossRef]

5. Yan, S.; Guo, H.; Liu, G.; Ruan, Z. Mountain glacier displacement estimation using a Dem-assisted Offset Tracking method with ALOS/PALSAR data. *Remote Sens. Lett.* **2013**, *4*, 494–503. [CrossRef]

6. Bartholomaus, T.C.; Anderson, R.S.; Anderson, S.P. Response of glacier basal motion to transient water storage. *Nature Geosci.* **2008**, *1*, 33–37. [CrossRef]

7. Ke, L.; Ding, X.; Song, C. Heterogeneous changes of glaciers over the Western Kunlun Mountains based on ICESat and Landsat-8 derived glacier inventory. *Remote Sens. Environ.* **2015**, *168*, 13–23. [CrossRef]

8. Khadka, D.; Babel, M.S.; Shrestha, S.; Tripathi, N.K. Climate change impact on glacier and snow melt and runoff in Tamakoshi basin in the Hindu Kush Himalayan (HKH) region. *J. Hydrol.* **2014**, *511*, 49–60. [CrossRef]

9. Nakamura, K.; Doi, K.; Shibuya, K. Fluctuations in the flow velocity of the Antarctic Shirase Glacier over an 11-year period. *Polar Sci.* **2010**, *4*, 443–455. [CrossRef]

10. Yasuda, T.; Furuya, M. Short-term glacier velocity changes at West Kunlun Shan, northwest Tibet, detected by synthetic aperture radar data. *Remote Sens. Environ.* **2013**, *128*, 87–106. [CrossRef]

11. Jiang, Z.-L.; Liu, S.-Y.; Peters, J.; Lin, J.; Long, S.-C.; Han, Y.-S.; Wang, X. Analyzing Yengisogat Glacier surface velocities with ALOS PALSAR data feature tracking, Karakoram, China. *Environ. Earth Sci.* **2012**, *67*, 1033–1043. [CrossRef]

12. Kumar, V.; Venkataraman, G.; Høgda, K.A.; Larsen, Y. Estimation and validation of glacier surface motion in the northwestern Himalayas using high-resolution SAR intensity tracking. *Int. J. Remote Sens.* **2013**, *34*, 5518–5529. [CrossRef]

13. Rignot, E.; Kanagaratnam, P. Changes in the velocity structure of the Greenland Ice Sheet. *Science* **2006**, *311*, 986–990. [CrossRef] [PubMed]

14. Rignot, E.; Mouginot, J.; Scheuchl, B. Ice flow of the Antarctic Ice Sheet. *Science* **2011**, *333*, 1427–1430. [CrossRef] [PubMed]

15. Riveros, N.; Euillades, L.; Euillades, P.; Moreiras, S.; Balbarani, S. Offset Tracking procedure applied to high resolution SAR data on Viedma Glacier, Patagonian Andes, Argentina. *Adv. Geosci.* **2013**, *35*, 7–13. [CrossRef]

16. Scherler, D.; Leprince, S.; Strecker, M. Glacier-surface velocities in alpine terrain from optical satellite imagery—Accuracy improvement and quality assessment. *Remote Sens. Environ.* **2008**, *112*, 3806–3819. [CrossRef]

17. Wang, P.; Li, Z.; Li, H.; Wang, W.; Wang, F. Ice surface-elevation change and velocity of Qingbingtan Glacier No.72 in the Tomor region, Tianshan mountains, Central Asia. *J. Mt. Sci.* **2011**, *8*, 855–864. [CrossRef]

18. Racoviteanu, A.E.; Williams, M.W.; Barry, R.G. Optical remote sensing of glacier characteristics: A review with focus on the Himalaya. *Sensors* **2008**, *8*, 3355–3383. [CrossRef]

19. Liu, L.; Jing, Z.; Du, J. A study of velocity of Baishui No.1 Glacier, Mt. Yulong. *Adv. Earth Sci.* **2012**, *7*, 987–992.

20. Saepuloh, A.; Koike, K.; Omura, M. Applying Bayesian decision classification to Pi-SAR polarimetric data for detailed extraction of the geomorphologic and structural features of an active volcano. *IEEE Geosci. Remote Sens. Lett.* **2012**, *9*, 554–558. [CrossRef]

21. Saepuloh, A.; Koike, K.; Urai, M.; Sumantyo, J.T.S. Identifying surface materials on an active volcano by deriving dielectric permittivity from polarimetric SAR data. *IEEE Geosci. Remote Sens. Lett.* **2015**, *12*, 1620–1624. [CrossRef]

22. Goldstein, R.M.; Engelhardt, H.; Kamb, B.; Frolich, R.M. Satellite radar interferometry for monitoring ice sheet motion: Application to an Antarctic Ice Stream. *Science* **1993**, *262*, 1525–1530. [CrossRef] [PubMed]

23. Gourmelen, N.; Kim, S.W.; Shepherd, A.; Park, J.W.; Sundal, A.V.; Björnsson, H.; Pálsson, F. Ice velocity determined using conventional and multiple-aperture InSAR. *Earth Planet. Sci. Lett.* **2011**, *307*, 156–160. [CrossRef]

24. Kenyi, L.; Kaufmann, V. Estimation of rock glacier surface deformation using SAR interferometry data. *IEEE Trans. Geosci. Remote Sens.* **2003**, *41*, 1512–1515. [CrossRef]

25. Jung, H.-S.; Won, J.-S.; Kim, S.-W. An improvement of the performance of multiple-aperture SAR interferometry (mai). *IEEE Trans. Geosci. Remote Sens.* **2009**, *47*, 2859–2869. [CrossRef]

26. Jung, H.-S.; Yun, S.-H.; Jo, M.-J. An improvement of multiple-aperture SAR interferometry performance in the presence of complex and large line-of-sight deformation. *IEEE J. Sel. Top. Appl. Earth Obs. Remote Sens.* **2015**, *8*, 1743–1752. [CrossRef]

27. Strozzi, T.; Luckman, A.; Murray, T.; Wegmuller, U.; Werner, C.L. Glacier motion estimation using SAR offset-tracking procedures. *IEEE Trans. Geosci. Remote Sens.* **2002**, *40*, 2384–2391. [CrossRef]

28. Raspini, F.; Moretti, S.; Fumagalli, A.; Rucci, A.; Novali, F.; Ferretti, A.; Prati, C.; Casagli, N. The COSMO-SkyMed Constellation monitors the Costa Concordia Wreck. *Remote Sens.* **2014**, *6*, 3988–4002. [CrossRef]

29. Paradella, W.R.; Ferretti, A.; Mura, J.C.; Colombo, D.; Gama, F.F.; Tamburini, A.; Santos, A.R.; Novali, F.; Galo, M.; Camargo, P.O.; et al. Mapping surface deformation in open pit iron mines of Carajás province (Amazon region) using an integrated SAR analysis. *Eng. Geol.* **2015**, *193*, 61–78. [CrossRef]

30. Raspini, F.; Ciampalini, A.; Del Conte, S.; Lombardi, L.; Nocentini, M.; Gigli, G.; Ferretti, A.; Casagli, N. Exploitation of amplitude and phase of satellite SAR images for landslide mapping: The case of Montescaglioso (South Italy). *Remote Sens.* **2015**, *7*, 14576–14596. [CrossRef]

31. Zhou, J.; Li, Z.; Guo, W. Estimation and analysis of the surface velocity field of mountain glaciers in Muztag ata using satellite SAR data. *Environ. Earth Sci.* **2013**, *71*, 3581–3592. [CrossRef]

32. Jarvis, A.; Reuter, H.I.; Nelson, A.; Guevara, E. Hole-Filled SRTM for the Globe Version 4, Available from the Cgiar-Csi SRTM 90 m Database. Available online: http://srtm.csi.cgiar.org (accessed on 23 July 2015).

33. Zhang, Z.; Jiao, K. Modern glaciers on the south slope of West Kunlun Mountains (in Aksayqin Lake and Guozha Co Lake drainage areas). *Bull. Glacier Res.* **1987**, *5*, 85–91.

34. Kang, X.; Xie, Y. The character of the weather and climate in the West Kunlun Mountains area in summer, 1987. *Bull. Glacier Res.* **1989**, *7*, 77–81.

35. Zhang, L.; Guo, H.; Ji, P.; Chen, J. A Research of Glacier Change in West Kunlun through Remote Sensing. In Proceedings of the 2012 IEEE International Geoscience and Remote Sensing Symposium, Munich Germany, 22–27 July 2012; pp. 4430–4433.

36. Yan, S.; Guo, H.; Liu, G.; Fu, W. Monitoring Muztagh Kuksai Glacier surface velocity with L-band SAR data in southwestern Xinjiang, China. *Environ. Earth Sci.* **2013**, *70*, 3175–3184. [CrossRef]

37. McMillan, M.; Shepherd, A.; Gourmelen, N.; Park, J.-W.; Nienow, P.; Rinne, E.; Leeson, A. Mapping ice-shelf flow with interferometric synthetic aperture radar stacking. *J. Glaciol.* **2012**, *58*, 265–277. [CrossRef]

38. Yun, S.-H.; Zebker, H.; Segall, P.; Hooper, A.; Poland, M. Interferogram formation in the presence of complex and large deformation. *Geophys. Res. Lett.* **2007**, *34*, L12305. [CrossRef]

39. Song, R.; Guo, H.; Liu, G.; Perski, Z.; Yue, H.; Han, C.; Fan, J. Improved Goldstein SAR interferogram filter based on adaptive-neighborhood technique. *IEEE Geosci. Remote Sens. Lett.* **2015**, *12*, 140–144. [CrossRef]

40. Chen, C.W.; Zebker, H.A. Phase unwrapping for large SAR interferograms: Statistical segmentation and generalized network models. *IEEE Trans. Geosci. Remote Sens.* **2002**, *40*, 1709–1719. [CrossRef]

41. Bechor, N.B.D.; Zebker, H.A. Measuring two-dimensional movements using a single InSAR pair. *Geophys. Res. Lett.* **2006**, *33*, L16311. [CrossRef]

42. Hu, J.; Li, Z.W.; Ding, X.L.; Zhu, J.J.; Zhang, L.; Sun, Q. 3D coseismic displacement of 2010 Darfield, New Zealand Earthquake estimated from multi-aperture InSAR and D-InSAR measurements. *J. Geod.* **2012**, *86*, 1029–1041. [CrossRef]

43. Strozzi, T.; Kouraev, A.; Wiesmann, A.; Wegmueller, U.; Sharov, A.; Werner, C. Estimation of Arctic glacier motion with satellite L-band SAR data. *Remote Sens. Environ.* **2008**, *112*, 636–645. [CrossRef]

44. Li, J.; Li, Z.-W.; Ding, X.-L.; Wang, Q.-J.; Zhu, J.-J.; Wang, C.-C. Investigating mountain glacier motion with the method of SAR intensity-tracking: Removal of topographic effects and analysis of the dynamic patterns. *Earth-Sci. Rev.* **2014**, *138*, 179–195. [CrossRef]